Kinetic and Modeling Study of the Ethylene Oxychlorination to 1,2-Dichloroethane in Fluidized-Bed Reactors

Andrea Montebelli,[†,§] Enrico Tronconi,[*,†] Carlo Orsenigo,[‡] and Nicola Ballarini[‡]

[†]Politecnico di Milano, Dipartimento di Energia, Via La Masa 34, 20156 Milano, Italy

[‡]Clariant Prodotti Italia, Via G. Fauser 36/B, 28100 Novara, Italy

Received: April 17, 2015
Revised: August 26, 2015
Accepted: September 8, 2015
Published: September 8, 2015

1. INTRODUCTION

Discovered in the 1930s and first commercialized in the late 1950s, ethylene oxychlorination is a well-known catalytic process aimed at reusing HCl formed in the thermal cracking (pyrolysis) of 1,2-dichloroethane (DCE) to give vinyl chloride (VCM) in the so-called *balanced process*.[1] In this way, direct chlorination of ethylene, DCE pyrolysis, and ethylene oxychlorination are coupled in a single process to increase the VCM throughput from ethylene and chlorine with no net consumption or production of HCl.

More specifically, in the oxychlorination reaction, ethylene, HCl, and air (or oxygen) react over a $CuCl_2/\gamma$-Al_2O_3 catalyst (8−16 wt % $CuCl_2$ in commercial formulations[2−4]) at 200−300 °C and 1−10 bar giving mostly DCE and water according to the following stoichiometry:[5]

$$C_2H_4 + 0.5O_2 + 2HCl \rightarrow C_2H_4Cl_2 + H_2O$$
$$\Delta H^0_{R,298K} = -295\ \text{kJ/mol} \quad (1)$$

The reaction is strongly exothermic, and a good temperature control is essential both to ensure high selectivities and to prevent rapid catalyst deactivation.[5] Indeed, onset of selectivity loss due to further oxychlorination and oxidation reactions is found above 240 °C,[1,6,7] the main byproducts being ethyl chloride (C_2H_5Cl), 1,1,2-trichloroethane ($C_2H_3Cl_3$), chloral (C_2Cl_3HO), carbon tetrachloride (CCl_4), chloroform ($CHCl_3$), CO, and CO_2.[8] Vinyl chloride, methyl chloride, methylene dichloride, chloroethanol, and dichloroethylene are also formed, but only in minor amounts. Moreover, temperature control is essential to limit the sublimation rate of copper chlorides, which are highly volatile species.[9−11]

It is almost generally agreed that the oxychlorination kinetic mechanism involves a redox process wherein copper cycles between the Cu^{2+} and Cu^{+} states, being periodically reduced by ethylene and reoxidized by oxygen.[5,6,12,13] The active site probably involves an isolated Cu_xCl_y complex which is anchored to the high-surface-area γ-Al_2O_3 support.[12,14−16]

The detailed chlorination mechanism generating such a wide variety of byproducts and determining the process selectivity, however, has not been clearly understood yet, likely being the result of a combination of parallel and successive oxychlorination and hydrochlorination steps.[6,17] An open debate still exists also about the origin of carbon oxides: under oxidative conditions in the absence of HCl, Zhernosek et al.[18] and Rossberg et al.[5] found that carbon oxides come from ethylene deep oxidation, whereas Gel'perin et al.[6] ascribe their formation to the combustion of DCE. However, this latter explanation is in contrast with other findings by Zhernosek et al.[18] who demonstrated that DCE is quite stable and is not transformed into other byproducts. Others[19,20] do not agree with such a chemical stability of DCE and state that this species is rather transformed into chloral, the latter being progressively oxidized to CO and, eventually, CO_2.

Concerning kinetic dependencies, there is good agreement in the open literature about the oxychlorination reaction rate dependence on the ethylene and oxygen partial pressures, whereas a zero-order dependence is found with respect to HCl.[2,14] Nevertheless, HCl strongly affects the selectivity to DCE, the latter being markedly decreased upon increasing the HCl partial pressure.[2] Interestingly, HCl is also found to inhibit the deep oxidation reactions.[18]

Industrially, the reaction is carried out in fixed- or fluidized-bed reactors, with oxygen being supplied as pure gas (oxygen-based process) or as conventional air (air-based process). The oxygen-based process operates with an excess of ethylene with respect to stoichiometric hydrogen chloride (C_2H_4/HCl = 0.53−0.59). This allows operating with lower temperatures which provide higher ethylene selectivities, because of the limited combustion rates and the higher DCE purity, and very high HCl conversions. The vent gas is recycled to the reactor after the condensation step, and only a small portion of the vent gas is purged (about 1/100 of that required for air-based processes[5]).

Fluidized-bed reactors are usually preferred because, despite the need of periodical makeup to compensate for the catalyst fraction lost in cyclones and its degradation due to mechanical friction, they provide effective reaction heat removal and very effective gas/solid mass and heat transfer thanks to the high gas circulation rate used to keep the bed in the fluidized state and to ensure an even catalyst distribution within the vessel. In contrast to fixed-beds, fluidized-bed reactors provide near isothermal operations, ruling out external mass- and heat-transfer limitations. Moreover, the use of fine (ca. 10−200 μm diameter[1]) catalyst powder reduces the risk of internal mass transport limitations as well, which are noticeable in contrast in fixed-bed reactors loaded with catalyst pellets having characteristic dimensions in the order of millimeters.

Accordingly, low byproducts selectivities are obtained and, thanks to their intrinsically safe design (i.e., third body suppression effect against radical chain propagation), the reaction can be carried out within the explosive limits, which makes feed control less critical.[5,21] However, attention should be paid to avoid sticky catalyst particles because catalyst agglomeration may lead to poor fluidization.[5]

Finding its root in the two-phase theory of Davidson and Harrison,[22] further developed by Kunii and Levenspiel[23] and by Werther,[24,25] modeling of fluidized-bed reactors has been extensively addressed in the chemical engineering literature for a wide range of industrial processes (e.g., methanation,[26] catalytic oxidation of *n*-butane to maleic anhydride,[27,28] ethane conversion to VCM[29]), highlighting the importance of fluid dynamics in determining the reactor performances.[30] In principle, Davidson and Harrison's simple two-phase (STP) theory assumes the fluidized-bed to consist of two distinct phases, namely, the bubble phase, mainly containing gas in the form of bubbles moving upward through the bed as a plug flow, and the emulsion phase, i.e., a well-mixed mixture of catalyst powder and gas. Chemical reactions are assumed to occur only in the emulsion phase, which is commonly modeled as a perfectly mixed tank reactor. Accordingly, reactants have to diffuse across the two phases before reaching the catalytically active sites. In this respect, being one of the most important parameters in determining the reactor fluid dynamics, bubble size has to be carefully controlled to ensure an effective diffusive transport.[7,30,31] It is worth noticing that, by assuming negligible throughflow of solids within the bed, the STP theory is usually valid only for fluidized-beds operating in the bubbling regime. In this regime, the relatively low gas velocities are not able to exert enough drag force on solids to cause a significant entrainment.[23]

Due to the typically high gas flow rates employed, however, industrial fluidized-bed reactors are often operated in the turbulent fluidization regime rather than in the bubbling one.[32] In this case, there is no longer distinction between phases, but only a single pseudohomogenous phase exists, moving upward the fluidized-bed basically as a "plug-flow", including a certain degree of mass axial dispersion, and containing the catalyst. Specifically, the axially dispersed plug-flow (ADPF) approximation becomes relevant when onset of turbulent fluidization is observed, i.e., when the gas superficial velocity, u_0, is greater than the transition velocity, u_c, given by the following correlation,[33] with symbols defined in Notation:

$$u_c = 0.57 Ar^{0.46} \mu_g / (\rho_g d_p) \tag{2}$$

Only a few papers in the literature are concerned with mathematical modeling of industrial oxychlorination fluidized-bed reactors.[7,31] Moreover, all of them adopt the "two-phase" assumption and implement very old and/or simplified kinetic models, providing a limited description of the reacting system. This hinders an accurate account of reactor performance in terms of selectivities to the most relevant byproducts, which is extremely important in the perspective of the optimization of process conditions and of the development of new oxychlorination catalyst formulations.

In this work we present a novel kinetic study of the ethylene oxychlorination reaction. In particular, we perform a DOE-based study of the intrinsic oxychlorination kinetics in a dedicated flow reactor loaded with a commercial $CuCl_2/\gamma$-Al_2O_3-based catalyst and propose a detailed oxychlorination kinetic model relying on 9 chemical reactions which accounts for the evolution of 12 species, including 6 byproducts, namely C_2H_5Cl, $C_2H_3Cl_3$, C_2Cl_3HO, a lumped pseudocomponent comprising C_1 chlorinated hydrocarbons, CO, and CO_2. We then estimate the related rate constants by multiresponse nonlinear regression of the experimental data.

In the second part of the paper we present the development and the validation against industrial data of two fluidized-bed reactor models, the former being based on the classical Davidson and Harrison STP theory and the latter describing the reactor according to the ADPF approximation. Both models incorporate the new intrinsic oxychlorination kinetics.

2. EXPERIMENTAL SECTION

The tubular flow reactor setup for the kinetic study included a feed section for reactant/inert gases (i.e., C_2H_4, O_2, HCl, and N_2) supplied as pure gases from certified cylinders. Each feed line was equipped with a mass flow controller (Brooks 5850S). In cofeed experiments, CO and CO_2 were fed through the N_2 line, whereas DCE and water were fed by means of a Jasco PU-2080 HPLC pump.

The reacting mixture entered a Hastelloy C tubular reactor (ID = 10.7 mm, L = 650 mm), which was inserted in an electric furnace (Carbolite VST 12/400). The reactor was loaded with a commercial $CuCl_2/\gamma$-Al_2O_3 oxychlorination catalyst powder (63−80 μm as particle size distribution, ρ_p = 1.52 g/cm^3), diluted (5:1 v/v) with graphite of similar size. The catalytic bed was located in the isothermal zone of the furnace and kept in place by two layers of corundum spheres (0.5−1 mm as diameter) placed at the top and at the bottom. The overall catalytic bed length was 8 cm, and the temperature profile was measured by a sliding multipoint thermocouple (OD = 3 mm) immersed in the bed.

All the lines were made of Hastelloy to prevent acidic attacks. Reactor inlet and outlet sections were kept at 200 °C by heating tapes to avoid condensations.

Once the gas mixture exited the reactor, it was expanded to atmospheric pressure by means of a back pressure controller (Precision Fluid, Badger Meter provided with Hastelloy C trim), then it passed through three condensation steps for the removal of DCE, H_2O, and unconverted HCl: the gas mixture was first cooled with well water, then with ethylene glycol refrigerated at −8 °C, and finally with dry ice at about −78 °C. The gas stream coming from the condenser was sent to a set of three traps (i.e., empty trap, $AgNO_3$, and Silica Gel) to remove all traces of H_2O and HCl. The off gases (i.e., N_2, O_2, CO, CO_2, and C_2H_4) were sent either to a gas flow meter (Ritter TG 05-7) or to an online GC (Agilent CP490), which also served to analyze the feed gas composition. Accordingly, C_2H_4, HCl, and O_2 molar conversions were calculated as

$$\text{Mol. conversion } \% = \frac{(F_i^{\text{in}} - F_i^{\text{out}})}{F_i^{\text{in}}} \cdot 100 \tag{3}$$

The aqueous and organic phases were separated using a separating funnel. The organic phase, collected over 5 h, was analyzed by an off-line GC (Agilent GC7890 equipped with a CP Sil 5CB column) to quantify the chlorinated impurities, using toluene as internal standard. In this regard, the fraction of unreacted C_2H_4 dissolved in the crude DCE was considered negligible. The aqueous phase was periodically weighed and titrated by placing a dedicated $AgNO_3$ trap downstream from the glass condenser. The trap contained $AgNO_3$ with a defined concentration to convert quantitatively the excess of HCl to AgCl. By back-titration of unconverted salt, it was possible to determine the exact amount of unconverted HCl. Minor amounts of carbonates dissolved in the aqueous phase were neglected.

The duration of each kinetic run was limited to 20 h to secure fresh catalyst performances and to avoid possible active phase losses due to the high volatility of copper chlorides, as extensively reported in the open literature.[9−11] Carbon, chlorine, and oxygen balances were evaluated as

$$\text{C, Cl, O}_{\text{balance}} = \frac{(F_{(\text{C,Cl,O})}^{\text{in}} - F_{(\text{C,Cl,O})}^{\text{offgas}} - F_{(\text{C,Cl,O})}^{\text{prod/byprod}})}{F_{(\text{C,Cl,O})}^{\text{in}}} \cdot 100 \tag{4}$$

Only runs with balance errors in the range ±5% were considered.

3. KINETIC STUDY

3.1. Kinetic Runs. In line with typical industrial operating conditions, we studied the kinetic effects of T, P, $y_{C_2H_4}^{\text{in}}$, and C_2H_4/HCl and C_2H_4/O_2 molar ratios within the ranges reported in Table 1. In particular, C_2H_4/HCl and C_2H_4/O_2 ratios were varied by changing HCl or O_2 molar fraction in the feed gas and balancing with N_2.

Table 1. Investigated Kinetic Variables and Their Ranges

variables	range	reference	units
T	200−260	230	°C
P	2−6	4	bara
$y_{C_2H_4}^{\text{in}}$	0.1−0.3	0.2	mol/mol
C_2H_4/HCl	0.5−0.75	0.62	mol/mol
C_2H_4/O_2	1.5−2.5	2	mol/mol

To keep reactant conversions at kinetically relevant values in all tests, the gas hourly space velocity (GHSV) was preliminarily set to 5000 Nl/h/kg_{cat}. However, a dedicated series of tests was also performed to investigate the GHSV effect in the range of 1000−8000 Nl/h/kg_{cat} at reference conditions.

A set of preliminary diagnostic runs was performed to check the presence of gas phase reactions and the pressure drop within the catalytic bed. Furthermore, we performed dedicated cofeed experiments to elucidate combustion pathways (feed = $C_2H_4 + O_2$, DCE + O_2, CO + O_2, $C_2H_5Cl + O_2$) and to check the kinetic effects of C_2H_4, O_2, HCl, DCE, H_2O, CO, and CO_2. We found that (1) on increasing GHSV, the selectivity of all the considered reaction products decreased, thereby suggesting a terminal product nature for these species; (2) no evidence of gas-phase reactions was detected at the selected operating conditions; (3) pressure drop was limited to less than 20% of the reactor inlet value; (4) C_2H_4 and CO burned to CO_2, whereas combustion of DCE did not occur to an appreciable extent; interestingly, C_2H_5Cl partly burned to an almost equimolar mixture of CO and CO_2, whereas some was converted into C_2H_4; (5) co-feed experiments instead pointed out negligible kinetic effects of DCE, H_2O, CO, and CO_2; (6) ethylene and oxygen exhibited a promoting effect on the reaction rates, whereas HCl inhibited the formation rates of DCE and of most of the byproducts.

The application of Mears's diagnostic criteria[34−36] evidenced negligible axial/radial dispersion, bypass as well as internal and external mass- and heat-transfer limitations. This validated the assumption of an ideal "plug-flow" description of the test reactor and assured that the kinetic runs were performed in a genuine chemical regime, even under the most severe investigated conditions.

The design of experiments (DoE) included a 4 + 1 2-level fractional factorial design to grant uniform coverage of the experimental space. In addition to the basic runs, 10 "spoke" runs were also planned to provide nonlinear information, and two replicated central runs were performed to check the data reproducibility. A total of 28 kinetic runs were thus performed and used for estimating the rate constants.

3.2. Kinetic Model. Preliminary results indicated that over 95% of the inlet carbon and chlorine was accounted for in the kinetic runs when describing the evolution of DCE, C_2H_5Cl, $C_2H_3Cl_3$, C_2Cl_3HO, CO, and CO_2. Data coming from industrial plants suggest a marked formation of C_1 chlorinated hydrocarbons as well, especially $CHCl_3$ and CCl_4. Accordingly, and with the scope of developing a tool capable of guiding process development and/or scale-up industrial activities, we decided to account for all these species in our kinetic study.

We implemented a "parallel" reaction scheme in which all the reaction products originate from ethylene conversion, except for C_2H_5Cl, which, in line with our preliminary investigations, was considered as an intermediate species, also subjected to deep oxidation. An overall rate expression was adopted to account for the formation of a lumped pseudocomponent including all the C_1 chlorinated hydrocarbons with the number of chlorine atoms ranging from 1 to 4.

The proposed kinetic scheme, including 12 species and 9 global chemical reactions, is summarized in Table 2.

All chemical reactions were considered to be irreversible, except for the ethylene hydrochlorination to C_2H_5Cl (R_2), being equilibrium limited in the investigated temperature range. In agreement with the preliminary results in section 3.1, first-

Table 2. Reaction Network and Rate Expressions Assumed for the Present Kinetic Study

rate no.	chemical reaction	rate expression [mol/g_{cat}/s]
1	$C_2H_4 + 0.5O_2 + 2HCl \rightarrow C_2H_4Cl_2 + H_2O$	$k_1 p_{C_2H_4} p_{O_2}^n \frac{p_{HCl}}{(1 + K_1 p_{HCl})^2}$
2	$C_2H_4 + HCl \leftrightarrow C_2H_5Cl$	$k_2 p_{C_2H_4} \frac{p_{HCl}}{1 + K_1 p_{HCl}} \left(1 - \frac{p_{C_2H_5Cl}}{p_{HCl} p_{C_2H_4} K_{eq,2}}\right)$
3	$C_2H_4 + O_2 + 3HCl \rightarrow C_2H_3Cl_3 + 2H_2O$	$k_3 p_{C_2H_4} p_{O_2}^n \frac{p_{HCl}}{(1 + K_1 p_{HCl})^2}$
4	$C_2H_4 + 2O_2 + 3HCl \rightarrow C_2Cl_3HO + 3H_2O$	$k_4 p_{C_2H_4} p_{O_2}^n \frac{p_{HCl}}{1 + K_1 p_{HCl}}$
5	$C_2H_4 + 2O_2 \rightarrow 2CO + 2H_2O$	$\frac{k_5 p_{C_2H_4} p_{O_2}^n}{1 + K_2 p_{HCl}}$
6	$C_2H_4 + 3O_2 \rightarrow 2CO_2 + 2H_2O$	$\frac{k_6 p_{C_2H_4} p_{O_2}^n}{1 + K_3 p_{HCl}}$
7	$CO + 0.5O_2 \rightarrow CO_2$	$\frac{k_7 p_{CO_2} p_{O_2}^n}{1 + K_3 p_{HCl}}$
8	$C_2H_5Cl + 3O_2 \rightarrow 2CO_2 + 2H_2O + HCl$	$\frac{k_8 p_{C_2H_5Cl} p_{O_2}^n}{1 + K_3 p_{HCl}}$
9	$C_2H_4 + (x-1)O_2 + 2xHCl \rightarrow 2C_1Cl_xH_{4-x} + (2x-2)H_2O$	$k_9 p_{C_2H_4} p_{O_2}^n \frac{p_{HCl}}{1 + K_1 p_{HCl}}$

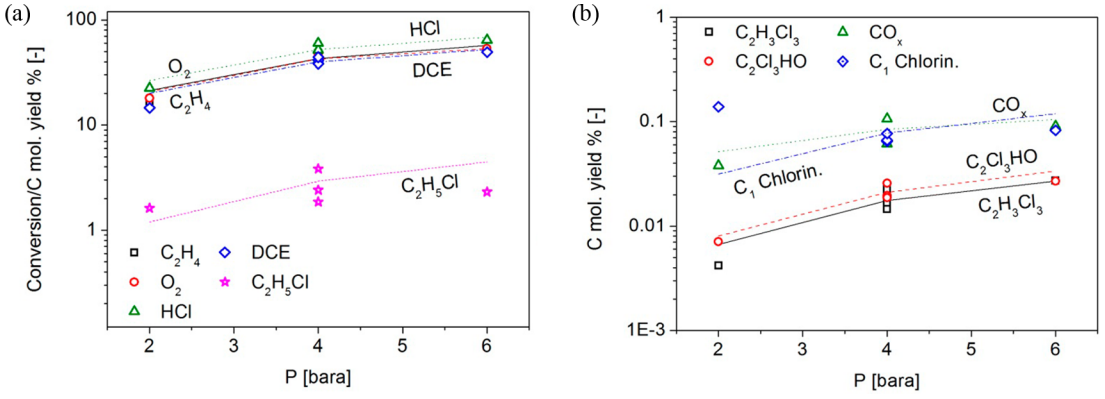

Figure 1. Effect of P on (a) reactant conversions, DCE and C_2H_5Cl yields, and (b) $C_2H_3Cl_3$, C_2Cl_3HO, C_1 chlorinated byproducts, and CO_x yields (T = 230 °C, $y^{in}_{C_2H_4}$ = 0.2, C_2H_4/HCl = 0.62, C_2H_4/O_2 = 2). Symbols: experimental data. Lines: model fit.

order dependencies with respect to C_2H_4 and variable orders with respect to O_2 were set. Concerning the HCl dependence, an inhibition term was introduced in the case of combustion rates (i.e., R_5, R_6, R_7, and R_8). DCE and $C_2H_3Cl_3$ production rates (i.e., R_1 and R_3) were properly corrected to take into account the HCl inhibition effect at the high HCl feed contents, whereas a first-order dependence was adopted at lower concentrations. C_2H_5Cl, C_2Cl_3HO, and C_1 chlorinated byproduct formation rates (i.e., R_2, R_4, and R_9) account for a zero-order dependence on HCl at high HCl contents and for a promoting effect at lower concentrations.

To reduce statistical correlation, rate constants k_j were written in the following Arrhenius reparameterized form:

$$k_j = \exp\left(\alpha_j - \beta_j \cdot \left(\frac{1000}{T} - \frac{1000}{T_{ref}}\right)\right) \quad (5)$$

where α_j and β_j are related to pre-exponential factors and activation energies as follows:

$$\alpha_j = \ln(k_j^0) - \frac{E_{act,j}}{1000 \cdot R \cdot T_{ref}} \quad (6)$$

$$\beta_j = \frac{E_{act,j}}{1000 \cdot R} \quad (7)$$

with the reference temperature, T_{ref}, being set to 230 °C.

Cut-off constants, K_1–K_3, were instead considered to be temperature-independent. A total of 20 adaptive parameters were therefore estimated by multiresponse nonlinear regression. According to the least-squares method, the objective function, SSE, was defined as follows:

$$SSE = \sum_{i=1}^{Nruns} \sum_{j=1}^{Nresp} (y_{i,j}^{exp} - y_{i,j}^{calc})^2 \quad (8)$$

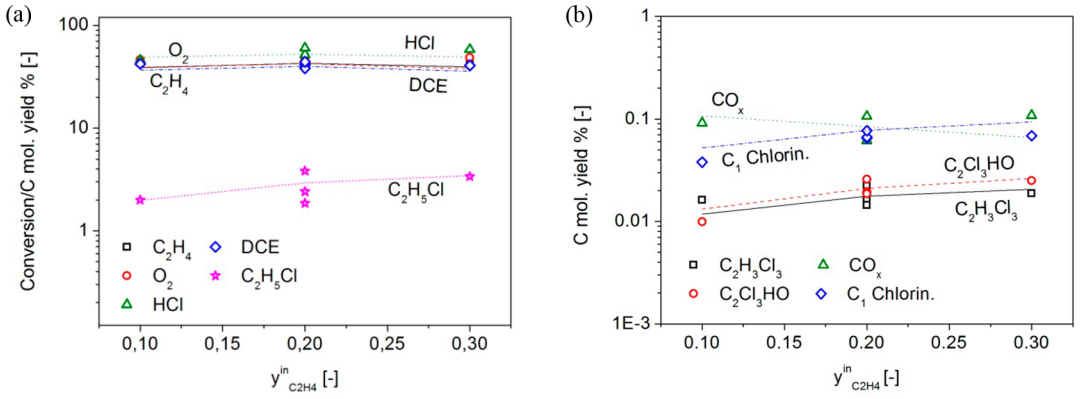

Figure 2. Effect of $y^{in}_{C_2H_4}$ on (a) reactant conversions, DCE and C_2H_5Cl yields, and b) $C_2H_3Cl_3$, C_2Cl_3HO, C_1 chlorinated byproducts, and CO_x yields (T = 230 °C, P = 4 bara, C_2H_4/HCl = 0.62, C_2H_4/O_2 = 2). Symbols: experimental data. Lines: model fit.

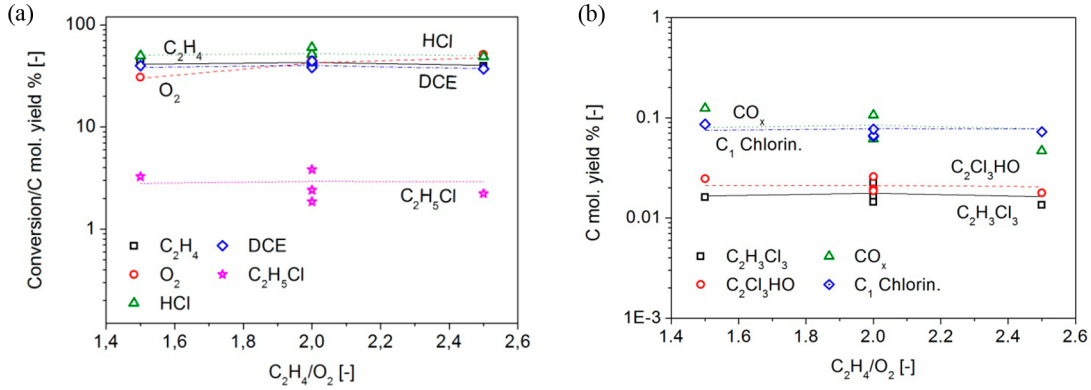

Figure 3. Effect of C_2H_4/O_2 on (a) reactant conversions, DCE and C_2H_5Cl yields, and b) $C_2H_3Cl_3$, C_2Cl_3HO, C_1 chlorinated byproducts, and CO_x yields (T = 230 °C, P = 4 bara, $y^{in}_{C_2H_4}$ = 0.2, C_2H_4/HCl = 0.62). Symbols: experimental data. Lines: model fit.

The minimization of SSE was accomplished by implementing and running a Newton−Gauss algorithm in a FORTRAN code. $y_{i,j}^{exp}$ and $y_{i,j}^{calc}$ represent the experimental and calculated carbon molar yields of species i with respect to ethylene in run j, respectively, evaluated as follows:

$$y_{i,j} = \frac{c_i \cdot F^{out}_{i,j}}{2 \cdot F^{in}_{C_2H_4,j}} \tag{9}$$

where c_i is the number of C atoms present in species i.

Calculated carbon molar yields were obtained by integration of a steady-state plug-flow model of the test reactor. The reactor was assumed isobaric, but not isothermal. Indeed, axial temperature gradients were not negligible in our runs, with hot-spots deviating by up to 10 °C from the average bed temperature at the most demanding conditions. Accordingly, a 5-point polynomial interpolation was included to provide an accurate representation of the axial temperature profile within the catalytic bed measured in each run.

Coherently, C_2H_4, HCl, and O_2 molar conversions were evaluated according to eq 3.

3.3. Analysis of Kinetic Data. The goodness of the kinetic fit is illustrated in Figures 1−5, which show experimental and calculated reactant conversions and product/byproduct carbon molar yields plotted against the investigated variables, i.e., T, P, $y^{in}_{C_2H_4}$, C_2H_4/HCl, and C_2H_4/O_2. In particular, CO and CO_2 are plotted as a single lumped pseudocomponent, named CO_x.

In spite of the marked standard deviation of replicated runs performed at reference conditions (i.e., 7.3% relative to the average DCE yield and 23.2% relative to the average $C_2H_3Cl_3$ yield), essentially due to the complexity of the analytical system, calculated values and their trends are in good accordance with the experimental evidence for most of the investigated conditions. In particular, pressure exhibits a marked promoting kinetic effect on all the molar yields, which is fairly well reproduced by the model (Figure 1). An exception is provided by C_1 chlorinated species, whose rate of formation is substantially unaffected by pressure. A moderate promoting effect of $y^{in}_{C_2H_4}$ is instead found on reactants conversion, DCE, $C_2H_3Cl_3$ and CO_x yields (Figure 2).

The same effect, though more marked, is seen also for C_2H_5Cl, C_2Cl_3HO, and C_1 chlorinated byproducts yields. Similar trends are found in the model predictions, even if with minor discrepancies in the case of CO_x. In particular, the CO_x yield is slightly underestimated at high ethylene feed contents.

For all the responses, a nearly flat dependence prevails with respect to the C_2H_4/O_2 feed ratio, except for the CO_x yield, which is strongly enhanced upon increasing the oxygen content in the feed stream (Figure 3).

Model predictions well describe the experimental results and only the CO_x yield is overestimated to some extent at high C_2H_4/O_2 ratios.

Slightly more pronounced dependences are found with respect to the C_2H_4/HCl feed ratio. In particular, as already reported,[2] HCl has an inhibitory effect on the DCE yield and,

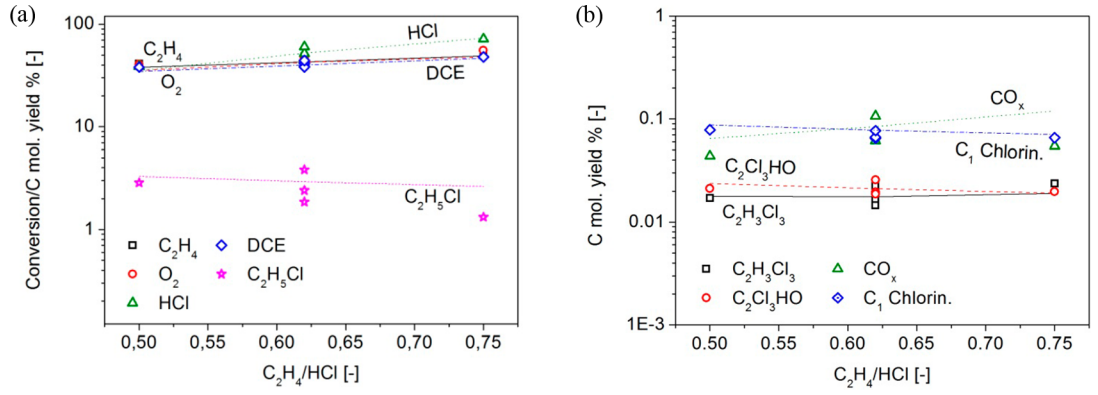

Figure 4. Effect of C_2H_4/HCl on (a) reactant conversions, DCE and C_2H_5Cl yields, and b) $C_2H_3Cl_3$, C_2Cl_3HO, C_1 chlorinated byproducts, and CO_x yields (T = 230 °C, P = 4 bara, $y^{in}_{C_2H_4}$ = 0.2, C_2H_4/O_2 = 2). Symbols: experimental data. Lines: model fit.

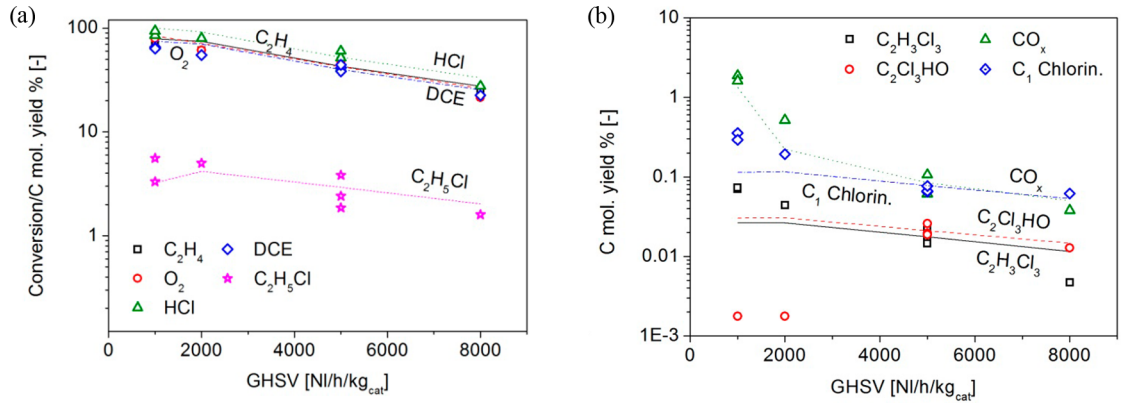

Figure 5. Effect of GHSV on (a) reactant conversions, DCE and C_2H_5Cl yields, and (b) $C_2H_3Cl_3$, C_2Cl_3HO, C_1 chlorinated byproducts, and CO_x yields (T = 230 °C, P = 4 bara, $y^{in}_{C_2H_4}$ = 0.2, C_2H_4/HCl = 0.62, C_2H_4/O_2 = 2). Symbols: experimental data. Lines: model fit.

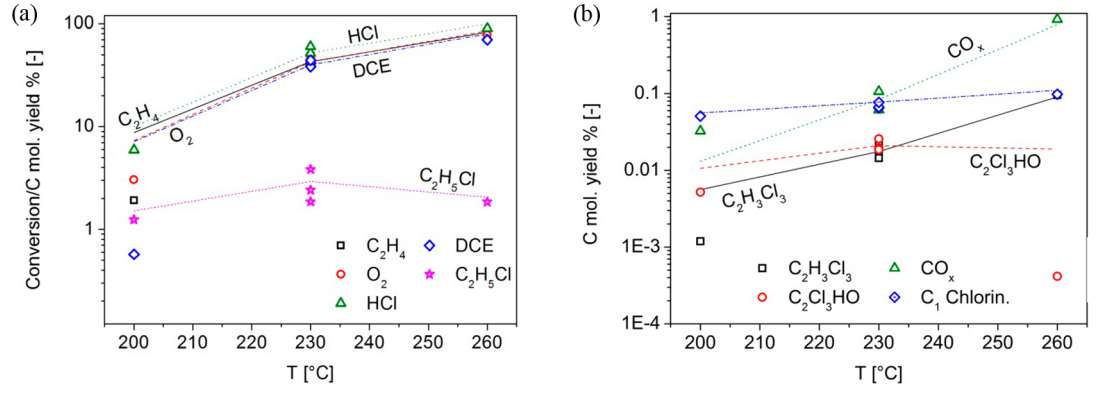

Figure 6. Effect of T on (a) reactant conversions, DCE and C_2H_5Cl yields, and (b) $C_2H_3Cl_3$, C_2Cl_3HO, C_1 chlorinated byproducts, and CO_x yields (P = 4 bara, $y^{in}_{C_2H_4}$ = 0.2, C_2H_4/HCl = 0.62, C_2H_4/O_2 = 2). Symbols: experimental data. Lines: model fit.

consequently, on the C_2H_4 and O_2 conversions, whereas it has a promoting effect on the C_2H_5Cl yield (Figure 4).

No significant effect of HCl is found instead on the $C_2H_3Cl_3$, C_2Cl_3HO, C_1 chlorinated byproducts, and CO_x yields. In particular, concerning this latter species, the experimental evidence is in contrast to that reported by the authors of ref 18, who observed an inhibition of HCl on the rates of the deep oxidation reactions. However, the promoting effect on the C_2H_5Cl yield could be reinterpreted as an inhibition of the C_2H_5Cl deep oxidation rate (R_8), therefore resulting in a greater accumulation of this byproduct in the reactor effluent.

Figure 5 shows the effect of GHSV, which basically confirms the "terminal product" behavior of DCE and of the other byproducts.

Higher reactant conversions, though still sufficiently far from unity, are found upon decreasing GHSV, except for HCl. Indeed, due to the slightly understoichiometric C_2H_4/HCl feed ratio employed at reference conditions, HCl is the limiting reactant and its conversions (both experimental and simulated ones) approach unity at the lowest space velocities, which explains also the plateau in the chlorinated byproducts yields. Interestingly, the experimental C_2Cl_3HO yield drops by 1 order of magnitude at GHSV = 2000 Nl/h/kg_{cat} and remains so low

also at 1000 Nl/h/kg_{cat}. As suggested also in refs 19 and 20, this effect may be due to a side combustion reaction not currently included in our kinetic model, which progressively oxidizes C_2Cl_3HO to CO and, eventually, to CO_2. However, the marked drop in the C_2Cl_3HO yield when moving from 5000 to 2000 Nl/h/kg_{cat} is rather suggestive of a problem in the analytical system, with the measured values for this species being very close to the gas chromatograph detection limit.

Concerning the temperature dependence, as expected, reactants conversions, DCE, and byproduct yields grow with increasing temperature: the model is able to satisfactorily reproduce such experimental trends (Figure 6).

Because C_2H_5Cl formation is an exothermic reaction limited by equilibrium, its net rate is penalized by high temperatures. At the same time, the C_2H_5Cl combustion rate is enhanced upon increasing the temperature, further contributing to the consumption of C_2H_5Cl and a decrease of its yield. This explains the maximum in the C_2H_5Cl yield shown in Figure 6a. It is noteworthy that the C_2Cl_3HO yield markedly drops at 260 °C, suggesting the presence of an additional side reaction, activated at higher temperatures, which quickly consumes such a species. As previously mentioned, this reaction may be an extra combustion reaction progressively transforming C_2Cl_3HO to CO and, eventually, CO_2 as proposed in refs 19 and 20.

The kinetic model slightly overestimates all the responses at the lower temperatures. Nevertheless, the estimated activation energy for the DCE formation rate ($E_{act,1}$ = 111.5 kJ/mol), whose simulated yield shows the largest deviation from the experimental data at low temperatures, resembles the estimates reported in previously published kinetic studies over similar catalysts.[2] Moreover, on assuming a typical $CuCl_2$ loading of 10 wt % and an average active phase dispersion of 45%,[11] the catalyst turnover frequency (TOF) is estimated to be about 0.36 h^{-1} at reference conditions, a value which is also in line with those found in previous studies.[2,17]

The parity plot in Figure 7 confirms the ability of the model to predict the DCE yield at the investigated conditions with relative errors below 10% in most of the runs, a value comparable with the average standard deviation of the experimental data. Moreover, all the kinetic parameters were found physically consistent and statistically significant at the 95% confidence level.

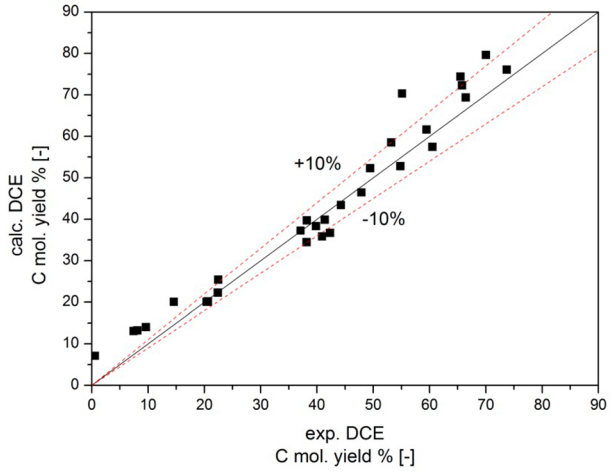

Figure 7. Parity plot for DCE yield, including ±10% limits.

4. FLUIDIZED-BED REACTOR MODELS

4.1. Simple Two-Phase Fluidized-Bed Reactor Model.

As widely used in the literature, Davidson and Harrison's simple two-phase model[22] has been adopted for modeling industrial oxychlorination fluidized-bed reactors. The model includes a series of assumptions, as summarized in the following:

1. The reactor is at steady-state.
2. The fluidized-bed is made of two distinct phases, i.e., a bubble and an emulsion phase.
3. The bubble phase is essentially made of gas moving upward through the bed in plug-flow, exchanging mass and heat with the emulsion phase along the catalytic bed.
4. The emulsion phase is assumed to be at minimum fluidizing conditions, perfectly mixed, and uniform in temperature: it contains gas and the catalyst. Here all the chemical reactions occur. This phase is described with a pseudohomogeneous approach, with the catalyst occupying a fraction of the emulsion phase total volume.
5. The mass-transfer resistances between the particles and the emulsion phase can be neglected, as well as the heat transfer between the emulsion and the bubble phase because the phenomenon is rapid enough to be considered at equilibrium.

Additionally, we neglect chemical transformations in the freeboard zone because of their minor importance. For simplicity, we do not consider the catalyst particle elutriation from the bed.

Mass and energy balance equations in the bubble phase and mass balance equations in the emulsion phase in accordance with the assumptions above are listed below as eqs 10−12.

Mass balances for the bubble phase

$$\begin{cases} \dfrac{\partial W_{i,b}}{\partial z} = -S_{free}\delta\rho_{g,b}K_{be,i}(\omega_{i,b} - \omega_{i,e}) \quad (i = 1, NC) \\ \text{at } z = 0,\ W_{i,b} = W_{i,b}^{in} \end{cases} \tag{10}$$

Energy balance for the bubble phase

$$\begin{cases} \dfrac{\partial T_b}{\partial z} = \dfrac{S_{free}\delta}{\sum_1^{NC} W_{i,b}C_{p,i,b}}[T_b \cdot \sum_{i=1}^{NC} C_{p,i,b}\rho_{g,b}K_{be,i} \\ \quad (\omega_{i,b} - \omega_{i,e}) - H_{be}(T_b - T_e)] \\ \text{at } z = 0,\ T_b = T_b^{in} \end{cases} \tag{11}$$

Mass balances for the emulsion phase

$$W_{i,e} = W_{i,e}^{in} + V_{tot}(1 - \delta)(1 - \varepsilon_{mf})MW_i\rho_p \sum_{j=1}^{NR} \nu_{ij}R_j + \int_0^Z S_{free}\delta\rho_{g,b}K_{be,i}(\omega_{i,b} - \omega_{i,e})\,dz \quad (i = 1, NC) \tag{12}$$

Model parameters, including those defining the reactor fluid dynamics, are provided in Table 3.

Gas flow splitting is crucial as it determines the fraction of gas rising through the bed as bubbles. If small particles and high flow rates are employed ($u_b \gg 5 \cdot u_{mf}/\varepsilon_{mf}$), gas flow splitting between the two phases can be evaluated as follows:[23]

$$u_0 = u_b \cdot \delta + u_{mf} \cdot (1 - \delta) \tag{26}$$

Table 3. Model Parameters

parameter	correlation	
void fraction at minimum fluidizing conditions[7]	$\varepsilon_{mf} = 0.586 \cdot \left(\frac{\mu_g^2}{\rho_g d_p^3 g(\rho_p - \rho_g)}\right)^{0.029} \cdot \left(\frac{\rho_g}{\rho_p}\right)^{0.021}$	(13)
gas velocity at minimum fluidization[7]	$u_{mf} = \frac{d_p^2(\rho_p - \rho_g)g}{1650\mu_g}, \quad Re_p < 20$	(14)
bubble velocity[37]	$u_b = 0.8 \cdot (u_0 - u_{mf}) + 0.71 \cdot 3.2 \cdot \sqrt{g d_b}$	(15)
bubble volume fraction[37]	$\delta = \frac{0.8 \cdot (u_0 - u_{mf})}{u_b}$	(16)
bubble size[38]	$d_{bm} = 2.59 g^{-0.2} \cdot \left[\frac{(u_0 - u_{mf})}{S_{tot}}\right]^{0.4}$	(17)
	$d_b = \frac{d_t}{4} \cdot \left(-\frac{2.56}{u_{mf}} \cdot \sqrt{\frac{d_t}{g}} + \sqrt{\left(\frac{2.56}{u_{mf}} \cdot \sqrt{\frac{d_t}{g}}\right)^2 + 4\frac{d_{bm}}{d_t}}\right)^2$	(18)
bubble−emulsion mass-transfer coefficients[23]	$\frac{1}{K_{be,i}} = \frac{1}{K_{bc,i}} + \frac{1}{K_{ce,i}}$	(19)
	$K_{bc,i} = 4.5\left(\frac{u_{mf}}{d_b}\right) + 5.85\left(\frac{D_i^{1/2} g^{1/4}}{d_b^{5/4}}\right)$	(20)
	$K_{ce,i} = 6.78\left(\frac{\varepsilon_{mf} D_i u_b}{d_b^3}\right)^{1/2}$	(21)
bubble−emulsion heat-transfer coefficients[23]	$\frac{1}{H_{be}} = \frac{1}{H_{bc}} + \frac{1}{H_{gp}}$	(22)
	$H_{bc} = 4.5\left(\frac{u_{mf}\rho_g C_{p,g}}{d_b}\right) + 5.85\frac{(k_g \rho_g C_{p,g})^{1/2} g^{1/4}}{d_b^{5/4}}$	(23)
	$H_{gp} = \gamma_b a_v h_{gp}$	(24)
	$h_{gp} = \frac{Nu_p k_g}{d_p}, \quad Nu_p = 2 + 0.6 Pr^{1/3} Re_p^{1/2}$	(25)

Because the bubble size is recognized as a key parameter in determining the reactor fluid dynamics, and therefore its performance,[30] a careful study was carried out to identify the most appropriate correlation for its evaluation. Being the adopted commercial catalyst of the Geldart A type,[39] Horio and Nonaka's correlation[38] was adopted (see eqs 17 and 18). Such a correlation provides an estimation of the equilibrium bubble size, d_b, which is established close to the distributor level, where the balance between the bubble coalescence and splitting frequencies is reached. It may be observed that this assumption was also used by Mostoufi et al.[27] in their simulation study of a fluidized-bed reactor for the catalytic oxidation of *n*-butane to maleic anhydride.

The reactor model was implemented in a FORTRAN code. A continuation algorithm was adopted for solution of the DAE system. Inlet mass flows (W_i^0) and reactor temperature and pressure (T_e, T_b^{in}, P) were the model input. Reactor geometry (d_t, S_{coils}), expanded bed density (ρ_b), and catalyst properties (d_p and ρ_p) were the model parameters. Outlet mass flows (W_i) and bubble temperature (T_b) were the output, as resulting from perfect gas mixing in the freeboard zone.

4.2. Axially Dispersed Plug-Flow Fluidized-Bed Reactor Model. When the fast fluidization regime applies ($u_0 > u_c$), there is no more distinction between bubble and emulsion phases, and all the gas flows through the bed as a plug-flow carrying the catalyst upward.[32] Due to the fast gas recirculation, the reactor can still be considered isothermal, but the transport resistances between the gas and solid phases become negligible. However, some back diffusion can occur and has to be included in the model. Accordingly, a more realistic approach is to adopt an axially dispersed plug-flow reactor model. The corresponding mass balance equations on the pseudohomogeneous phase are listed below as eq 27.

Mass balances for the pseudohomogeneous gas phase

$$\begin{cases} \frac{dW_i}{dz} = S_{free} MW_i (1 - \varepsilon)\rho_p \sum_{j=1}^{NR} \nu_{ij} R_j + S_{free} MW_i D_{z,i} \frac{d^2 C_i}{dz^2} \\ \quad (i = 1, NC) \\ @z = 0, \quad \frac{dW_i}{dz} = -\frac{W_i - W_i^{in}}{S_{free} \frac{\rho_g}{W_{tot}} D_{z,i}} \\ @z = L, \frac{dW_i}{dz} = 0 \end{cases} \quad (27)$$

where the effective axial diffusivity $D_{z,i}$ was evaluated according to the following correlation:[40]

$$Pe_{ax,i} = u_0 L / D_{z,i} = 0.247 Ar^{0.32} (D_t/d_p)^{0.02344} Sc_i^{-0.2317} \quad (28)$$

In such a model, all the gas flows through the reactor carrying the catalyst upward with a velocity u_0 and eq 26 collapses into the limiting case of $\delta = 0$. It is noteworthy that the determination of the bubble size is no longer required and the reactor fluid dynamics is entirely governed by the gas volumetric fraction, ε which can be evaluated as follows:

$$\varepsilon = 1 - \frac{\rho_{bed}}{\rho_p} \tag{29}$$

Numerical integration of the ordinary differential equations system in eq 27, forming a boundary-value problem, was accomplished by orthogonal collocation techniques. The same input and output of the STP model were used.

4.3. Validation of Reactor Models against Industrial Data. The previously developed kinetic mechanism was included in both reactor models, which were then validated against industrial data coming from two full-scale oxychlorination fluidized-bed reactors loaded with the same catalyst type used for the kinetic study (Table 4). The two reactors mainly differ in the vessel size, feed composition, and GHSV: in particular, the second reactor has a larger vessel diameter and is operated at lower C_2H_4/HCl and C_2H_4/O_2 feed molar ratios and at higher GHSV with respect to the first reactor. However, both reactors are operated at nearly the same superficial velocity, u_0, which is almost double the transition velocity, u_c. Therefore, according to the Bi and Grace criterion[33] (eq 2), they should operate in the same fluid dynamic regime, namely the turbulent fluidization regime.

Table 4. Model Input and Reactor Parameters for Two Different Industrial Oxychlorination Fluidized-Bed Reactors

variables	unit	industrial reactor no. 1	industrial reactor no. 2
d_t	cm	276	405
T_e	°C	230.8	235.3
T_b^{in}	°C	148.1	135.4
P	bara	4.7	5.1
$y_{C_2H_4}^{in}$	mol/mol	0.19	0.18
C_2H_4/HCl	mol/mol	0.55	0.52
C_2H_4/O_2	mol/mol	1.92	1.69
Q_{tot}^{in}	Nl/h	19.15×10^6	46.03×10^6
d_p	μm	50	50
ρ_p	g/cm^3	1.52	1.52
GHSV	Nl/h/kg$_{cat}$	594	719
u_0	m/s	0.43	0.48
u_c	m/s	0.23	0.22

The two industrial reactors were simulated by running both the STP and the ADPF model in a predictive mode. The results are shown in Table 5, which compares experimental and calculated reactants molar conversions and product/byproducts carbon molar yields per pass. Inspection of Table 5 indicates that the STP model significantly underestimates the activity of the two reactors, in terms of both reactants conversion and DCE yield. This can be explained by the continuously stirred tank reactor (CSTR) assumption adopted for the emulsion phase, where the chemical reactions occur. According to a CSTR behavior, indeed, the catalyst experiences the lowest reactant concentrations, namely those occurring at the reactor outlet, and this provides the slowest reaction rates.

On the other hand, in the ADPF model, the plug-flow assumption better approximates the reactor fluid dynamics dictated by the turbulent fluidization regime, in which the high gas velocity causes the solids to be entrained by the gas flow, both moving up the reactor in a plug flow. Accordingly, the catalyst experiences on the average reactant concentrations throughout the catalytic bed higher than those of a CSTR, therefore enhancing the overall reactor activity. As a result, the ADPF model provides better predictions than the STP model. However, the overall reactor activity is still underestimated.

The effective axial diffusivity, $D_{z,i}$, predicted by a semi-empirical correlation (eq 28), was identified as a possible source of uncertainty. In this regard, it has to be noted that the estimate of $D_{z,i}$, representing the extent of the mass axial dispersion phenomenon within the reactor, could significantly affect the model predictions, as it would reduce or emphasize the reactor plug-flow behavior.

Accordingly, a parametric study was performed to assess this effect, with results shown in Table 6. Unsurprisingly, on reducing $D_{z,i}$, therefore moving toward a more pronounced plug-flow behavior, the model provides predictions better in line with the experimental performances of both the industrial reactors. Specifically, a 7-fold reduction of $D_{z,i}$ was required to fit the reactor performances in terms of reactants conversions and DCE yield. Simulated O_2 conversion still remains lower than the experimental one, and this could be ascribed to underestimation of the CO_x yields. The rate of formation of C_2 chlorinated byproducts is overestimated as well.

It is worth noting that in the industrial practice the oxychlorination catalyst is typically subjected to iron contaminations due to the periodic impingement of the catalyst particles on the reactor wall.[41] In addition to their proven catalytic activity in the formation of polymeric species, which may damage the mechanical properties of the catalyst causing increased pressure drop and poor fluidization,[41] iron impurities have been found to reduce the catalyst lifetime and activity/selectivity.[42] Specifically, oxidation reactions of chlorinated byproducts are typically enhanced. We therefore performed a

Table 5. Comparison between STP and ADPF Models in Reproducing Experimental Data from the Two Industrial Reactors of Table 4

		industrial reactor no. 1			industrial reactor no. 2		
		exptl	STP model	ADPF model	exptl	STP model	ADPF model
conversion %	C_2H_4	91.23	83.47	89.35	96.19	80.67	93.04
	O_2	95.21	79.75	85.16	92.03	67.23	78.55
	HCl	99.17	90.17	96.27	99.59	82.68	95.33
C mol. yield %	DCE	88.41	80.21	85.39	92.47	77.32	89.30
	C_2 chlorinated byprod.	0.44	2.62	3.22	0.29	2.90	3.04
	C_1 chlorinated byprod.	0.11	0.09	0.11	0.16	0.08	0.10
	CO_x	1.60	0.52	0.58	2.53	0.31	0.55

Table 6. Simulation of Industrial Reactors with ADPF Model: Parametric Study on $D_{z,i}$ and Pre-exponential Factors k_2 and k_8

		industrial reactor no. 1				industrial reactor no. 2			
		exptl	ADPF model	ADPF model ($D_{z,i}$/7)	ADPF model ($D_{z,i}$/7, k_2/3.8, k_8·21.5)	exptl	ADPF model	ADPF model ($D_{z,i}$/7)	ADPF model ($D_{z,i}$/7, k_2/3.8, k_8·21.5)
conversion %	C_2H_4	91.23	89.35	92.66	91.71	96.19	93.04	96.43	95.86
	O_2	95.21	85.16	89.59	95.64	92.03	78.55	82.02	87.68
	HCl	99.17	96.27	99.17	99.31	99.59	95.33	98.30	98.72
C mol. yield %	DCE	88.41	85.39	87.64	89.57	92.47	89.30	91.75	93.87
	C_2 chlorinated byprod.	0.44	3.22	3.86	0.24	0.29	3.04	3.67	0.22
	C_1 chlorinated byprod.	0.11	0.11	0.14	0.14	0.16	0.10	0.13	0.14
	CO_x	1.60	0.58	0.95	1.68	2.53	0.55	0.80	1.56

parametric study by introducing a multiplier to the pre-exponential factors k_j in the rate expressions of the reactions R_2 and R_8 in the direction of reduced C_2H_5Cl production rate, typically one of the most abundant byproducts, as well as increased C_2H_5Cl oxidation rate. Table 6 shows the results of this study, which identifies k_2 divided by 3.8 and k_8 multiplied by 21.5 as the best fit. As expected, an increased C_2H_5Cl oxidation rate not only provided a more reasonable prediction of the CO_x yield but also contributed to increase the O_2 conversion, getting closer to the industrial data.

On the whole, the performances of both reactors are fairly well-reproduced by the ADPF model with the adjusted parameters, except for the slightly underestimated oxygen consumption to give CO_x in the second reactor. Nevertheless, considering also the great scaling factor ($\approx 10^6$) existing between the lab scale setup used for the intrinsic kinetic study and the simulated industrial units, the reactor model accuracy can be considered satisfactory.

5. CONCLUSIONS

We have developed a new kinetic model for the ethylene oxychlorination reaction, which includes 9 chemical reactions and describes the evolution of 12 species (including 6 major byproducts). Twenty adaptive rate constants were estimated by multiresponse nonlinear regression of experimental data collected from a systematic campaign of intrinsic kinetic tests performed over a commercial $CuCl_2/\gamma$-Al_2O_3 catalyst and planned according to a composite fractional factorial design.

The kinetic model so developed was able to reproduce the DCE yield with relative errors below 10% in most of the kinetic runs, a value comparable with the average standard deviation of the experimental data. Moreover, all the kinetic parameters were found physically consistent and statistically significant at the 95% confidence level.

We then derived two mathematical models of oxychlorination fluidized-bed reactors, namely the simple two-phase and the axially dispersed plug-flow models. The former one, based on the Davidson and Harrison theory, was found unsuitable for reproducing the experimental data coming from two full-scale industrial units, whose performances were substantially underpredicted by the STP model. On assuming instead a plug-flow reactor behavior, which is more consistent with the fluid dynamics of industrial units typically operating in the turbulent fluidization regime, the ADPF model provided better predictions.

Tuning of the effective mass axial diffusivity, in the direction of less effective back mixing and more pronounced plug-flow reactor behavior, granted further refined predictions of reactants conversions and DCE yields.

Description of byproduct distribution was eventually adjusted by tuning the rate constants (i.e., pre-exponential factors) of C_2H_5Cl production and oxidation reactions. This is justified considering the iron contamination typically affecting the commercial catalysts due to the periodic strikes of the catalyst particles against the reactor wall, which is known to alter the activity/selectivity of the catalytic process.

AUTHOR INFORMATION

Corresponding Author

*E-mail: enrico.tronconi@polimi.it Phone: +39 02 2399 3264.

Present Address

§A.M.: Lamberti SpA, Corporate Engineering, via Piave 18, 21041 Albizzate (VA), Italy.

Notes

The authors declare no competing financial interest.

ACKNOWLEDGMENTS

The authors from Politecnico di Milano gratefully acknowledge funding by Clariant International Ltd. This study is part of the Clariant effort devoted to the continuous understanding and performance improvement of its catalysts.

NOTATION

a_v = catalyst particle surface-to-volume ratio [m^{-1}]
$Ar = ((d_p^3 \rho_G(\rho_S - \rho_G)g)/\mu_G^2)$ = Archimedes number [−] c_i = number of C atoms present in species i [−]
$C_{p,g}$ = gas mixure specific heat [J/mol/K]
$C_{p,i}$ = gas specific heat of species i [J/mol/K]
C_2H_4/HCl = ethylene-to-hydrogen chloride inlet molar ratio [−]
C_2H_4/O_2 = ethylene-to-oxygen inlet molar ratio [−-]
d_b = average bubble size [m]
d_{bm} = maximum bubble size [m]
d_p = catalyst particle diameter [m]
d_t = reactor diameter [m]
D_i = molecular diffusion coefficient of species i [m^2/s] D_{ij} = binary diffusion coefficient of species i in species j [m^2/s]
$D_{z,i}$ = effective axial diffusivity of species i [m^2/s]
$E_{act,j}$ = activation energy for reaction j [J/mol]
F_i = gas molar flow rate of species i [mol/s]
GHSV = gas hourly space velocity [$Nl/h/kg_{cat}$]
g = gravitational acceleration [m/s^2]
h_{gp} = gas−particle heat-transfer coefficient [$cal/cm^2_{catalyst}/s$]

H_{bc} = bubble−cloud heat-transfer coefficient [cal/$cm^3_{bubbles}$/s]
H_{be} = bubble−emulsion heat-transfer coefficient [cal/$cm^3_{bubbles}$/s]
H_{gp} = gas−particle heat-transfer coefficient [cal/$cm^3_{bubbles}$/s]
k_g = gas thermal conductivity [W/m/K]
k_j = kinetic constant for reaction j
k_j^0 = pre-exponential factor for reaction j
K_1,K_2,K_3 = cutoff constants [$bara^{-1}$]
$K_{bc,i}$ = bubble−cloud mass-transfer coefficient of species i [$cm^3_{gas}/cm^3_{bubbles}$/s]
$K_{ce,i}$ = bubble−emulsion mass-transfer coefficient of species i [$cm^3_{gas}/cm^3_{bubbles}$/s]
$K_{ce,i}$ = cloud−emulsion mass-transfer coefficient of species i [$cm^3_{gas}/cm^3_{bubbles}$/s]
$K_{eq,2} = \exp(16.085 - (8772.1/T))$ = equilibrium constant for ethylene direct chlorination reaction to ethyl chloride [−]
L = expanded bed height [m]
MW_i = molecular weight of species i [kg/mol]
NC = number of components [−]
P = pressure [bara]
$Pe_{ax,i}$ = axial Péclet number of species i [−]
$Pr = ((\mu_g C_{p,g})/k_g)$ = Prandtl number [−]
Q_{tot} = total gas flow rate [Nl/h]
R = gas constant [J/mol/K]
R_j = reaction rate j [mol/g_{cat}/s]
$Re_p = ((d_p \rho_g u_0)/u_g)$ = Reynolds number [−]
S_{tot} = reactor cross section [m^2]
S_{coils} = cooling coils cross section [m^2]
S_{free} = free reactor cross section [m^2]
Sc_i = Schmidt number of species i ($= \mu_g/\rho_g/D_i$) [−]
T = temperature [K]
u_0 = gas superficial velocity [m/s]
u_b = bubble velocity [m/s]
u_c = transition velocity [m/s]
V_{tot} = reactor volume [m^3]
W_{cat} = catalyst load [g]
W_i = gas mass flow rate of species i [kg/s]
W_{tot} = total gas mass flow rate [kg/s]
y_i = molar fraction of species i [−]
z = reactor axial coordinate [m]

Greek Symbols

α_j = reparameterized pre-exponential factor for reaction j [−]
β_j = reparameterized activation energy for reaction j [K]
γ_b = catalyst volumetric fraction in bubbles [$m^3_{cat}/m^3_{bubbles}$]
δ = bubbles volumetric fraction [$m^3_{bubbles}/m^3_{reactor}$]
ε = gas volumetric fraction [$m^3_{gas}/m^3_{reactor}$]
μ_g = gas mixture dynamic viscosity [Pa·s]
μ_i = dynamic viscosity of species i [Pa·s]
ν_{ij} = stoichiometric coefficient of species i in reaction j [-]
ρ_f = expanded bed density [kg_{bed}/m^3_{bed}]
ρ_g = gas mixture density [kg_{gas}/m^3_{gas}]
ρ_p = catalyst particle density [kg_{cat}/m^3_{cat}]
ω_i = mass fraction of species i [−]

Subscripts

$_e$ = referred to the emulsion phase
$_b$ = referred to the bubble phase
$_{mf}$ = minimum fluidizing conditions

Superscripts

^{in} = at reactor inlet
$^{off\ gas}$ = contained in the off gas
^{out} = at reactor outlet
$^{prod/byprod}$ = contained in product and byproducts

REFERENCES

(1) Magistro, A. J.; Cowfer, J. A. Real world of industrial chemistry: Oxychlorination of ethylene. *J. Chem. Educ.* **1986**, *63*, 1056.
(2) Carrubba, R. V.; Spencer, J. L. Kinetics of the oxychlorination of ethylene. *Ind. Eng. Chem. Process Des. Dev.* **1970**, *9*, 414.
(3) Wachi, S.; Asai, Y. Kinetics of 1,2-dichloroethane formation from ethylene and cupric chloride. *Ind. Eng. Chem. Res.* **1994**, *33*, 259.
(4) Lamberti, C.; Prestipino, C.; Bonino, F.; Capello, L.; Bordiga, S.; Spoto, G.; Zecchina, A.; Diaz Moreno, S.; Cremaschi, B.; Garilli, M.; Marsella, A.; Carmello, D.; Vidotto, S.; Leofanti, G. The Chemistry of the Oxychlorination Catalyst: an In Situ, Time-Resolved XANES Study. *Angew. Chem., Int. Ed.* **2002**, *41*, 2341.
(5) Rossberg, M.; Lendle, W.; Pfleiderer, G.; Tögel, A.; Dreher, E.-L.; Langer, E.; Rassaerts, H.; Kleinschmidt, P.; Strack, H.; Cook, R.; Beck, U.; Lipper, K.-A.; Torkelson, T. R.; Löser, E.; Beutel, K. K.; Mann, T. Chlorinated Hydrocarbons. In *Ullmann's Encyclopedia of Industrial Chemistry*; Wiley-VCH Verlag GmbH & Co.: Weinheim, 2000.
(6) Gel'perin, E. I.; Bakshi, Y. M.; Zyskin, A. G.; Snagovskii, Y. S.; Avetisov, A. K. Kinetics and Mechanism of Ethylene Oxychlorination. *Russian Chemical Industry* **1996**, *28*, 38.
(7) Moreira, J. C. S.; Pires, C. A. M. Modelling and simulation of an oxychlorination reactor in a fluidized bed. *Can. J. Chem. Eng.* **2010**, *88*, 350.
(8) Chlorocarbons and Chlorohydrocarbons. In *Kirk-Othmer Encyclopedia of Chemical Technology*, 5th ed.; John Wiley and Sons, Inc.: New York, 2007; Vol. *6*, pp 12−17.
(9) Mallikarjunan, M. M.; Zahed Hussain, S. Oxychlorination of Some Lower Aliphatic Hydrocarbons. *J. Sci. Ind. Res.* **1983**, *42*, 209.
(10) Forzatti, P.; Lietti, L. Catalyst deactivation. *Catal. Today* **1999**, *52*, 165.
(11) Muddada, N. B.; Olsbye, U.; Leofanti, G.; Gianolio, D.; Bonino, F.; Bordiga, S.; Fuglerud, T.; Vidotto, S.; Marsella, A.; Lamberti, C. Quantification of copper phases, their reducibility and dispersion in doped-CuCl2/Al2O3 catalysts for ethylene oxychlorination. *Dalton Transactions* **2010**, *39*, 8437.
(12) Arganbright, R. P.; Yates, W. F. Chlorination with cupric chloride. *J. Org. Chem.* **1962**, *27*, 1205.
(13) Prasad, P. S. S.; Prasad, K. B. S.; Ananth, M. S. Parameter estimation in a fixed-bed reactor operating under unsteady state: Oxychlorination of ethylene. *Ind. Eng. Chem. Res.* **2001**, *40*, 5487.
(14) Zhernosek, V. M.; Vasil'eva, I. B.; Avetisov, A. K.; Gel'bshtein, A. I. Kinetics and mechanism of the catalytic oxidative chlorination of ethylene. *Kinet. Katal.* **1971**, *12*, 353.
(15) Naworski, J. S.; Velez, E. S. Oxychlorination of ethylene. *Appl. Ind. Catal.* **1983**, *1*, 239.
(16) Chen, F.; Yang, Y.; Rong, S.; Chen, G. Studies on ethylene oxychlorination II. Reaction mechanism and kinetics. *J. Petrochem. Eng.* **1994**, *23*, 421.
(17) Avetisov, A. K.; Ostrovsky, G. M.; Snagovsky, Y. S.; Zyskin, A.
(18) FBREAC User Guide. http://www.nifhi.ru/ru/subdivision/chemical_kinetics/chim_kinet/fbreac/default.aspx#ancMain (accessed April 3, 2014).
(18) Zhernosek, V. M.; Vasil'eva, I. B.; Avetisov, A. K.; Gel'bshtein, A. I. Kinetics of the side reaction of the hydroxychlorination process of ethylene. *Kinet. Katal.* **1973**, *14*, 690.
(19) Flid, M. R.; Kurlyandskaya, I. I.; Dmitriev, Y. K.; Babotina, M. V. The formation of carbon oxides in the ethylene oxidative chlorination process in the presence of copper chloride catalysts. In *CHISA '98*, Praha, **1998**.
(20) Legutke, G.; Rechmeier, G. H.; Scholz, H.; Schuchardt, K.; Höller, E.; Liesenfelder, G. Production of 1,2-dichloroethane. U.S. Patent 4,310,713, 1982.
(21) Smallwood, P. V.; Stephenson, M. W.; Newman, M. W.; Bunten, I. J. Vinyl Chloride Polymers. In *Encyclopedia of Polymer Science and Engineering*, 2nd ed.; Kroschwitz, J. I., Ed.; Wiley: New York, 1989.
(22) Davidson, J. F.; Harrison, D. *Fluidised Particles*. Cambridge University Press: Cambridge, 1963.

(23) Kunii, D.; Levenspiel, O. *Fluidization Engineering*. John Wiley & Sons, Inc.: New York, 1969.
(24) Werther, J. Mathematical modeling of fluidized bed reactors. *Int. Chem. Eng.* **1980**, *20*, 529.
(25) Werther, J. Scale-up modeling for fluidized bed reactors. *Chem. Eng. Sci.* **1992**, *47*, 2457.
(26) Kopyscinski, J.; Schildhauer, T. J.; Biollaz, S. M. A. Methanation in a fluidized bed reactor with high initial CO partial pressure: Part II-Modeling and sensitivity study. *Chem. Eng. Sci.* **2011**, *66*, 1612.
(27) Mostoufi, N.; Cui, H.; Chaouki, J. A comparison of two- and single-phase models for fluidized-bed reactors. *Ind. Eng. Chem. Res.* **2001**, *40*, 5526.
(28) Dente, M.; Pierucci, S.; Tronconi, E.; Cecchini, M.; Ghelfi, F. Selective oxidation of n-butane to maleic anhydride in fluid bed reactors: Detailed kinetic investigation and reactor modelling. *Chem. Eng. Sci.* **2003**, *58*, 643.
(29) Hickman, D. A.; Jones, M. E.; Jovanovic, Z. R.; Olken, M. M.; Podkolzin, S. G.; Stangland, E. E.; Thompson, R. K. Reactor scale-up for fluidized bed conversion of ethane to vinyl chloride. *Ind. Eng. Chem. Res.* **2010**, *49*, 10674.
(30) Karimipour, S.; Pugsley, T. A critical evaluation of literature correlations for predicting bubble size and velocity in gas-solid fluidized beds. *Powder Technol.* **2011**, *205*, 1.
(31) Al-Zahrani, S. M.; Aljodai, A. M.; Wagialla, K. M. Modelling and simulation of 1,2-dichloroethane production by ethylene oxychlorination in fluidized-bed reactor. *Chem. Eng. Sci.* **2001**, *56*, 621.
(32) Thompson, M. L.; Bi, H.; Grace, J. R. A generalized bubbling/turbulent fluidized-bed reactor model. *Chem. Eng. Sci.* **1999**, *54*, 2175.
(33) Bi, H. T.; Grace, J. R. Effects of measurement method on velocities used to demarcate the onset of turbulent fluidization. *Chemical Engineering Journal* **1995**, *57*, 261.
(34) Mears, D. E. Diagnostic criteria for heat transport limitations in fixed bed reactors. *J. Catal.* **1971**, *20*, 127.
(35) Froment, G. F.; Bischoff, K. B.; De Wilde, J. *Chemical Reactor Analysis and Design*, 3rd ed.; John Wiley & Sons, Inc.: New York, 2010.
(36) Anderson, J. R.; Pratt, K. C. *Introduction to Characterization and Testing of Catalysts*. Academic Press: Sydney, 1985.
(37) Werther, J.; Hartge, E.-U. Modeling of Industrial Fluidized-Bed Reactors. *Ind. Eng. Chem. Res.* **2004**, *43*, 5593.
(38) Horio, M.; Nonaka, A. A. A Generalized Bubble Diameter Correlation for Gas-Solid Fluidized Beds. *AIChE J.* **1987**, *33*, 1865.
(39) Geldart, D. Types of gas fluidization. *Powder Technol.* **1973**, *7*, 285.
(40) Bi, H. T.; Grace, J. R. *Axial dispersion and interphase transfer in turbulent fluidized beds*; Fluidization Research Centre, University of British Columbia, Vancouver, Canada, 1997.
(41) Aharoni, C.; Inbar, J. Loss of copper from oxychlorination catalysts. *J. Appl. Chem. Biotechnol.* **1973**, *23*, 333.
(42) Campbell, R. G. Purification of feed gas streams containing ferric chloride in oxychlorination. U.S. Patent 4,000,205, 1976.